

# Spin Asymmetries of the Nucleon Experiment

Whitney R. Armstrong\* and Second Author†  
*Authors' institution and/or address*  
*This line break forced with \\*

Charlie Author‡  
*Second institution and/or address*  
*This line break forced and*  
*Third institution, the second for Charlie Author*

Delta Author  
*Authors' institution and/or address*  
*This line break forced with \\*

(SANE Collaboration)  
(Dated: January 7, 2016)

The Spin Asymmetries of the Nucleon experiment (SANE) measured two double spin asymmetries using a polarized proton target and polarized electron beam at two beam energies, 4.7 GeV and 5.9 GeV. A large acceptance, open configuration detector package identified scattered electrons at  $40^\circ$  and covered a wide range in Bjorken  $x$  ( $0.3 < x < 0.8$ ). The twist-3 matrix element,  $\tilde{d}_2^p$ , was extracted from the measured spin structure functions,  $g_1^p$  and  $g_2^p$ , that provides information on the dynamical higher twists associated with quark-gluon correlations. Our results at  $Q^2$  values from 1.0 to 6.0 GeV<sup>2</sup> were found to be in agreement with the two existing measurements and lattice QCD calculations, however, the scale dependence indicates observation of an average color Lorentz force.

Quantum chromodynamics successfully describes many observables in high energy processes where the coupling is small and perturbative (pQCD) calculations are applicable. Lattice QCD calculations continue to mature and provide insight when the coupling is strong. However, experiment and lattice calculations have had a dichotomous existence; lattice QCD calculations have great difficulty with experimentally-accessible observables, whereas, lattice easily calculates observables that are, at present, practically impossible to measure.

When promoted from subject of experimental investigation to theoretical tool, precision pQCD calculations are useful for unraveling the non-perturbative dynamics of color confinement. An operator product expansion (OPE) provides well-defined quantities which codify not only parton distributions, but also quark-gluon correlations that lack a partonic interpretation. Perhaps more importantly, a transversely polarized nucleon target probed with polarized electrons yields an *unique* experimental situation where non-trivial ab initio lattice QCD calculations can be tested.

The nucleon spin structure functions,  $g_1$  and  $g_2$ , parameterize the asymmetric part of the hadronic tensor, which through the optical theorem, is related to the forward virtual Compton scattering amplitude,  $T_{\mu\nu}$ . The reduced matrix elements of the quark operators appearing in the OPE analysis of  $T_{\mu\nu}$  are related to Cornwall-Norton (CN) moments of the spin structure functions. At next-to-leading twist, the CN moments of give

$$\int_0^1 x^{n-1} g_1(x, Q^2) dx = a_n + \mathcal{O}\left(\frac{M^2}{Q^2}\right), \quad n = 1, 3, \dots \quad (1)$$

and

$$\int_0^1 x^{n-1} g_2(x, Q^2) dx = \frac{n-1}{n} (d_n + a_n) + \mathcal{O}\left(\frac{M^2}{Q^2}\right), \quad (2)$$
$$n = 3, 5, \dots$$

where  $a_n = \tilde{a}_{n-1}/2$  and  $d_n = \tilde{d}_{n-1}/2$  are the twist-2 and twist-3 reduced matrix elements, respectively, which for increasing values of  $n$  have increasing dimension and spin.

If target mass corrections (TMCs) are neglected, the twist-3 matrix element can be extracted from the  $n = 3$  CN moments at fixed  $Q^2$

$$\tilde{d}_2 = \int_0^1 x^2 (2g_1(x) + 3g_2(x)) dx = 3 \int_0^1 x^2 \bar{g}_2(x) dx \quad (3)$$

where

$$\begin{aligned} \bar{g}_2(x) &= g_2(x) - g_2^{WW}(x) \\ &= g_2(x) - \left[ \int_x^1 \frac{g_1(y)}{y} dy - g_1(x) \right]. \end{aligned} \quad (4)$$

The term in brackets is the leading twist piece of  $g_2$  known as Wandzura-Wilczek (WW) relation [1], thus, leaving  $\bar{g}_2$  only containing higher twist contributions.

The  $\tilde{d}_2$  matrix element is of particular interest because it can be interpreted as an average transverse color Lorentz force acting on the struck quark the instant after being struck by the virtual photon[2, 3]. This can be easily seen by explicitly writing the matrix element

$$\tilde{d}_2 = \frac{1}{2MP^{+2}S^x} \langle P, S | \bar{q}(0) g G^{+y}(0) \gamma^+ q(0) | P, S \rangle. \quad (5)$$

where the proton is moving in the infinite momentum frame, i.e.,  $\vec{v} = -c\hat{z}$ , and the field strength tensor comes

$$\left[\vec{E} + \vec{v} \times \vec{B}\right]^y = E_y + B_x = \sqrt{2}G^{+y} \quad (6)$$

and

$$\begin{aligned} F^y &= -\frac{\sqrt{2}}{2P^+} \langle P, S | \bar{q}(0)G^{+y}(0)\gamma^+q(0) | P, S \rangle \\ &= -2M^2 d_2 \end{aligned} \quad (7)$$

Furthermore, when considering higher twist matrix elements Burkardt [2] showed that the color electric and magnetic forces can be separated by

$$F_E = \frac{-M^2}{4} \left[ \frac{2}{3}(2\tilde{d}_2 + \tilde{f}_2) \right] \quad (8)$$

$$F_B = \frac{-M^2}{2} \left[ \frac{1}{3}(4\tilde{d}_2 - \tilde{f}_2) \right]. \quad (9)$$

The twist-4 matrix element is defined as

$$\tilde{f}_2 M^2 S^\mu = \frac{1}{2} \sum_i e_i^2 \langle P, S | g \bar{\psi}_i \tilde{G}^{\mu\nu} \gamma_\nu \psi_i | P, S \rangle \quad (10)$$

and it can be extracted from the first moment of  $g_1$ . The next-to-leading twist contribution to  $\Gamma_1$  is written in terms of the reduced matrix elements[4]

$$\mu_4 = \frac{M^2}{9} \left( \tilde{a}_2 + 4\tilde{d}_2 + 4\tilde{f}_2 \right), \quad (11)$$

where  $\tilde{a}_2$  is twist-2,  $\tilde{d}_2$  is twist-3, and  $\tilde{f}_2$  is twist-4. Since  $\mu_4$  does not enter at leading twist it must be determined by subtracting the, presumably well known, leading twist

$$\Delta\Gamma_1 = \Gamma_1 - \mu_2 \quad (12)$$

where the  $\Delta\Gamma_1$  contains *all* higher twists. Therefore it should be clear that a clean determination of  $\tilde{f}_2$  would require precision data taken at high  $Q^2$  in order to make sure all higher twists are suppressed. Then by moving to lower  $Q^2$  the with matched precision in  $\tilde{d}_2$  and  $\tilde{a}_2$  the difference can be attributed to  $\tilde{f}_2$  or even higher twists. Before this can be done, however, the leading twist terms must be well determined by precision measurements at low  $x$ , where the integral of the first moment dominates and large momentum transfers to ensure the absence of higher twists.

It should be emphasized here that a measurement of  $g_2$  provides *direct* access to higher twist effects, i.e., without complicating fragmentation functions that are found in SIDIS experiments. This puts polarized DIS in an entirely unique situation to test lattice QCD [5] and model calculations of higher twist effects.

We conducted the experiment at Jefferson Lab in Hall C during the winter of 2008-2009 using a longitudinally

polarized electron beam and a polarized proton target. Production data was taken with two beam energies, 4.7 and 5.9 GeV, and with two target polarization directions: longitudinal, where the polarization direction was along the direction of the electron beam, and transverse, where the target polarization pointed in a direction perpendicular to the electron beam. The target angle for the transverse configuration was  $80^\circ$  in order to accommodate electrons detection at similar kinematics for both configurations. Scattered electrons were detected in a new detector stack called the big electron telescope array (BETA) and also independently in Hall-C's high momentum spectrometer (HMS).

The beam polarization was measured periodically using a Møller polarimeter and production runs had beam polarizations from 60% up to 90%. The beam helicity was flipped from parallel to anti-parallel at 30 Hz and the helicity state, determined at the injector, was recorded for each event.

A dynamically polarized ammonia target acted as an effective polarized proton target and achieved an average polarization of 68% by using a 5.1 T polarizing field and microwave pumped cryogenic target cells. NMR measurements, calibrated against the calculable thermal equilibrium polarization, provided a continuous monitor of the target polarization. To mitigate its local heating and depolarizing effects, the beam current was limited to 100 nA and a slow raster system moved the beam around within a 2 cm diameter circle. In order to allow for continuous taking, alternating target cells were used and swapped out of the beam when the polarization dipped below 60%. Also by adjusting the microwave pumping frequency the polarization direction was reversed. These two directions, positive and negative target polarizations, were used to estimate associated systematic uncertainties, and by taking equal amounts of data under positive and negative target polarization directions, cancel any correlated behavior in the sum. The initial data was taken with the target polarizing magnet in the transverse configuration then physically rotated into the longitudinal configuration.

BETA comprised of four detectors: a forward tracker placed close to the target, a threshold gas Cherenkov counter, a Lucite hodoscope, and a large electromagnetic calorimeter called BigCal. BETA was placed at a fixed central scattering angle of  $40^\circ$  and covered a solid angle of roughly 200 msr. Electrons were identified by the Cherenkov counter which had an average signal of roughly 20 photoelectrons[6]. The energy was determined by the BigCal calorimeter which consisted of 1744 lead glass blocks placed 3.5 m from the target. BigCal was calibrated using a set of  $\pi^0 \rightarrow \gamma\gamma$  events. The Lucite hodoscope provided additional timing and position event selection cuts and the forward tracker was not used in the analysis of production runs.

The target's 5.1 T polarizing magnetic field caused

large deflections for charged particle tracks. In order to reconstruct tracks at the primary scattering vertex, corrections to the momentum vector reconstructed at BigCal were calculated from a set of neural networks that were trained with simulated data sets for each configuration.

BETA's large solid angle and open configuration allowed a broad kinematic range in  $x$  and  $Q^2$  to be covered. The data was grouped into four  $Q^2$  bins to calculate the moments at nearly constant  $Q^2$ . The  $Q^2$  bins had average values of 1, 2, 3.5, and 4.5  $\text{GeV}^2/c^2$ .

The measured double spin asymmetries for longitudinal and transverse target polarizations were formed by changing the electron beam helicity and defined as

$$A_m(\alpha) = \frac{1}{df(W, Q^2)P_B P_T} \left[ \frac{N_+ - N_-}{N_+ + N_-} \right] \quad (13)$$

where  $\alpha = 180^\circ$  or  $80^\circ$  for the longitudinal and transverse target configurations respectively. The normalized counting rates are  $N_\pm = n_\pm / (Q_\pm L_\pm)$  where  $n_\pm$  is the raw number of counts,  $Q_\pm$  is the accumulated charge for the given beam helicity over the counting period, and  $L_\pm$  is the live time for each helicity,  $df(W, Q^2)$  is the target dilution factor, and the beam and target polarizations are  $P_B$  and  $P_T$  respectively.

The target dilution factor takes into account scattering from unpolarized nucleons in the target and is depends on the electron scattering kinematics. The packing fraction of the ammonia beads inside the target cell gives the relative amount of ammonia to liquid He inside and is crucial for an accurate determination of  $df$ . The packing fraction was determined by comparing the electron yields measured by the HMS to a simulation and using a carbon target with a well-known packing fraction to provide a baseline and calibration point for the simulation.

The major source of background comes from the decay of  $\pi^0$ s into two photons which, subsequently, produce an electron-positron pair that is then identified then as a DIS electron. Pairs produced outside outside of the target no longer experience a strong magnetic field and travel in nearly the same direction. These events produced twice the amount of Cherenkov light and are effectively removed with an upper ADC cut[6]. However, pairs produced inside the target are sufficiently deflected causing BETA to observe only one of the pairs' particles. These events cannot be removed through selection cuts and dominate the background events.

The background dilution and contamination was determined by fitting existing data and running a simulation to determine their relative contribution. This correction only becomes significant at energies below 1.2 GeV where the positron-electron ratio begins to rise. The background correction consisted of a dilution and contamination term defined as

$$A_b(\alpha) = A_m/f_{BG} - C_{BG}. \quad (14)$$

The contamination term was small and only increases to 1% at the lowest  $x$  bin. The background dilution increases with decreasing values of  $x$  and becomes significant ( $> 10\%$  of the measured asymmetry) only for  $x < 0.35$ .

After correcting for the pair symmetric background the radiative corrections were applied following the standard formalism laid out by Mo and Tsai [7] and the polarization dependent treatment of Akushevich, et.al. [8]. The elastic radiative tail calculated from models of the proton form factor [9]. The pair-symmetric background corrected asymmetry was corrected with elastic dilution and contamination terms

$$A_e(\alpha) = A_{cor}/f_{el} - C_{el} \quad (15)$$

where  $f_{el}$  is the ratio of inelastic scattering to the sum of elastic and inelastic scattering, and  $C_{el}$  is the elastic scattering cross section difference over the total inelastic cross section. The elastic dilution term remained less than 10% of the measured asymmetry in the range  $x = [0.3, 0.8]$  for both target configurations. In the same range of  $x$  the longitudinal elastic contamination remained less than 10% in absolute value, whereas, the transverse elastic contamination remained less than a few percent in absolute units.

The virtual Compton scattering asymmetries can be written in terms of the measured asymmetries

$$A_1 = \frac{1}{D(1 + \eta\xi)} \left[ A_{180}(1 + \chi \cot \alpha) + A_{80}(\chi \csc \alpha) \right] \quad (16)$$

$$A_2 = \frac{\xi - (\chi/\eta) \cot \alpha}{D(1 + \eta\xi)} \left[ A_{180} + A_\alpha \left( \frac{1}{\cos \alpha - \chi \sin \alpha \cos^2 \phi} \right) \right] \quad (17)$$

where  $\eta$ ,  $\xi$ , and  $\chi$  are functions of only the scattered electron kinematic variables, and  $D$  which also depends on the ratio of longitudinal to transverse cross section,  $R = \sigma_L/\sigma_T$ .

The spin structure functions can be obtained from the measured asymmetries by using equations 16 and 17 with

$$g_1 = \frac{F_1}{1 + \gamma^2} (A_1 + \gamma A_2) \quad (18)$$

$$g_2 = \frac{F_1}{1 + \gamma^2} (A_2/\gamma - A_1) \quad (19)$$

where  $\gamma^2 = Q^2/\nu^2$ . The combined results for  $g_1^p$  and  $g_2^p$  are shown in FIG. 1. These results significantly improve the world data on  $g_2^p$ . Additionally, it provides much needed data for both spin structure functions at high  $x$ .

When target mass corrections become significant matrix elements of definite twist and spin cannot be extracted from the CN moments. Nachtmann moments,

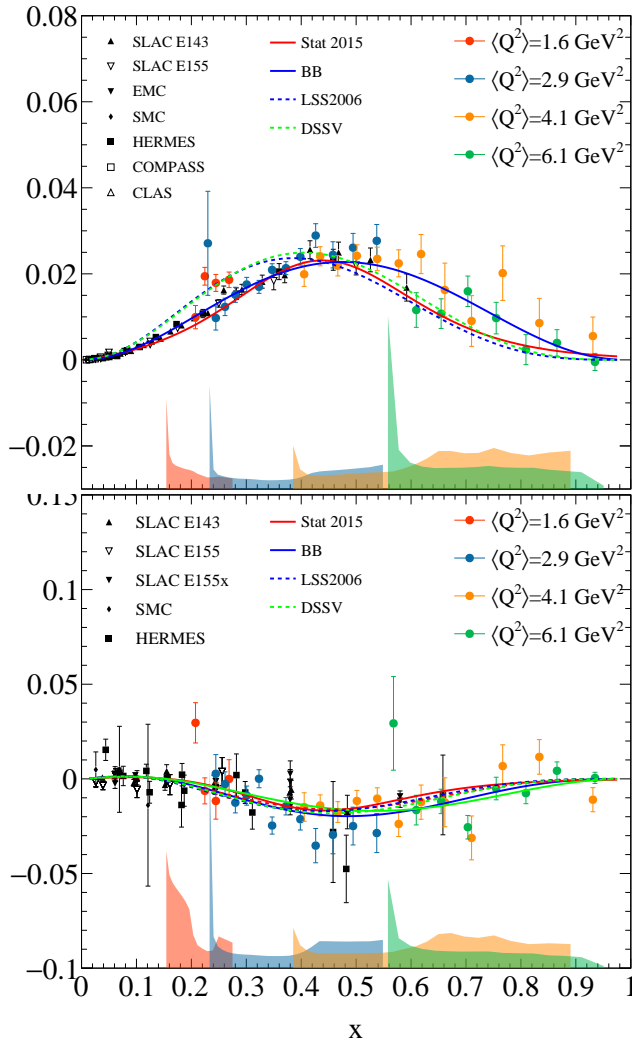


FIG. 1. The results for  $x^2 g_1^p$  (top) and  $x^2 g_2^p$  (bottom). (This is a place holder figure that will be improved)

by their construction, select matrix elements of definite twist and spin. At low  $Q^2$ , Nachtmann moments should be used instead of the CN moments as emphasized in [10]. Definitions of the Nachtmann moments are found in [10–12] and are related to the reduced matrix elements through

$$M_1^{(n)}(Q^2) = a_n = \frac{\tilde{a}_{n-1}}{2}, \quad \text{for } n = 1, 3, \dots \quad (20)$$

$$M_2^{(n)}(Q^2) = d_n = \frac{\tilde{d}_{n-1}}{2}, \quad \text{for } n = 3, 5, \dots \quad (21)$$

where we use the convention of Dong[13]. When the target mass is neglected, i.e.  $M^2/Q^2 \rightarrow 0$ , these equations reduce to  $M_1^1 = \Gamma_1$  and  $I = 2M_2^3$ .

It is important to note that the moments include the point at  $x = 1$  which corresponds to elastic scattering on the nucleon. Using empirical fits to the electric and magnetic form factors the elastic contribution to the mo-

ments is computed using the structure functions

$$g_1^{el}(x, Q^2) = \delta(x-1)G_M(Q^2) \frac{G_E(Q^2) + \tau G_M(Q^2)}{2(1+\tau)} \quad (22)$$

$$g_2^{el}(x, Q^2) = \delta(x-1)\tau G_M(Q^2) \frac{G_E(Q^2) - G_M(Q^2)}{2(1+\tau)} \quad (23)$$

where  $\tau = Q^2/4M^2$ . At large  $Q^2$  the elastic contribution is negligible. In some sense the elastic contribution,  $\tilde{d}_2^{el}$ , is of little interest; it is the deviation from the elastic, i.e. the inelastic part, which provides the insight into the color forces responsible for confinement.

The results for the Nachtmann moment  $2M_2^{(3)}(Q^2) = \tilde{d}_2(Q^2)$  are shown in FIG. 2 along with a comparison to the existing measurements and lattice calculations. The results around  $Q^2 = 5 \text{ GeV}^2$  are roughly in agreement with the lattice calculations [5].

The two previous measurements of  $\tilde{d}_2^p$  are shown in FIG. 2. The first  $\tilde{d}_2^p$  measurement at  $Q^2 = 5 \text{ GeV}^2$  was extracted from the combined results of the SLAC E143, E155, and E155x experiments[14]. The measurement from the Resonance Spin Structure (RSS) experiment [15, 16], extracted a value  $\tilde{d}_2^p$  value at  $Q^2 = 1.28 \text{ GeV}^2$ . These two results are shown in Figure 2 along with a lattice QCD calculation [17].

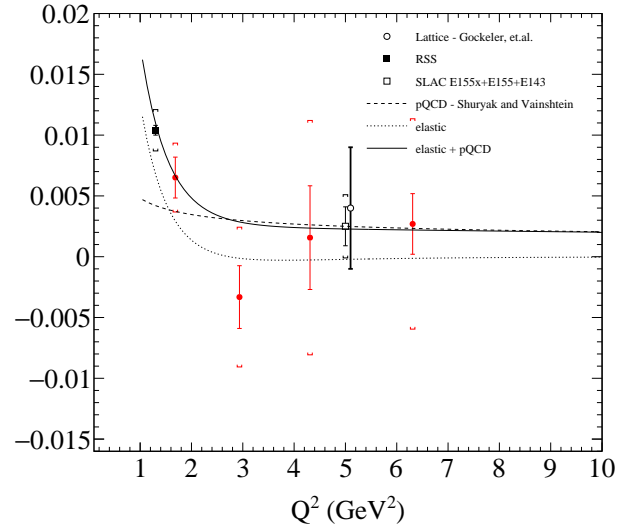


FIG. 2. The results for  $d_2^p$ . (This is a place holder figure that will be improved)

The results given in table I are consistent with previous measurements and lattice calculations, however, at intermediate  $Q^2$   $\tilde{d}_2$  is lower than the next-to-leading power corrections predict. Interestingly, this result is consistent with a recent neutron  $\tilde{d}_2^n$  measurement [18] which also observed a significantly more negative value

at  $Q^2 = 3 \text{ GeV}^2$ , indicating that the forces observed are iso-spin independent. Interpreted as an average color Lorentz force, this observation agrees with simple model that the proton and neutron, differing only by an iso-spin rotation, have the same color-space wave-function, therefore, on average the struck quark will feel the same color force.

In summary, the proton's spin structure functions  $g_1$  and  $g_2$  have been measured at kinematics allowing for an extraction of four  $\tilde{d}_2$  values each at near constant  $Q^2$ .

We wish to acknowledge the support of the author community in using REVTeX, offering suggestions and encouragement, testing new versions, . . .

---

\* Also at Physics Department, XYZ University.

† Second.Author@institution.edu

‡ <http://www.Second.institution.edu/~Charlie.Author>

[1] S. Wandzura and F. Wilczek, Phys. Lett. **B72**, 195 (1977).  
 [2] M. Burkardt, *Spin structure at long distance. Proceedings, Workshop, Newport News, USA, March 12-13, 2009*, AIP Conf. Proc. **1155**, 26 (2009), arXiv:0905.4079 [hep-ph].  
 [3] M. Burkardt, in *Exclusive reactions at high momentum transfer. Proceedings, 4th Workshop, Newport News, USA, May 18-21, 2010* (2011) pp. 101–110, arXiv:1009.5442 [hep-ph].  
 [4] X.-D. Ji and W. Melnitchouk, Phys. Rev. **D56**, 1 (1997), arXiv:hep-ph/9703363 [hep-ph].  
 [5] M. Gockeler, R. Horsley, W. Kurzinger, H. Oelrich, D. Pleiter, P. E. L. Rakow, A. Schafer, and G. Schierholz, Phys. Rev. **D63**, 074506 (2001), arXiv:hep-lat/0011091 [hep-lat].  
 [6] W. R. Armstrong, S. Choi, E. Kaczanowicz, A. Lukhanin,

Z.-E. Meziani, and B. Sawatzky, Nucl. Instrum. Meth. **A804**, 118 (2015), arXiv:1503.03138 [physics.ins-det].  
 [7] L. W. Mo and Y.-S. Tsai, Rev. Mod. Phys. **41**, 205 (1969).  
 [8] I. V. Akushevich and N. M. Shumeiko, J. Phys. **G20**, 513 (1994).  
 [9] J. Arrington, W. Melnitchouk, and J. A. Tjon, Phys. Rev. **C76**, 035205 (2007), arXiv:0707.1861 [nucl-ex].  
 [10] Y. B. Dong, Phys. Rev. **C78**, 028201 (2008), arXiv:0811.1002 [hep-ph].  
 [11] S. Matsuda and T. Uematsu, Nucl. Phys. **B168**, 181 (1980).  
 [12] A. Piccione and G. Ridolfi, Nucl. Phys. **B513**, 301 (1998), arXiv:hep-ph/9707478 [hep-ph].  
 [13] Some authors define the matrix elements excluding a factor of  $1/2$  [11, 19–21], and/or use even  $n$  for the moments [22, 23]. In this work we use the convention of [10, 12] which absorbs the  $1/2$  factor into the matrix element and use odd  $n$  for the moments, whereas, the matrix elements excluding the  $1/2$  and even  $n$  are  $\tilde{a}_{n-1}$  and  $\tilde{d}_{n-1}$ .  
 [14] P. L. Anthony *et al.* (E155), Phys. Lett. **B553**, 18 (2003), arXiv:hep-ex/0204028 [hep-ex].  
 [15] F. R. Wesselmann *et al.* (RSS), Phys. Rev. Lett. **98**, 132003 (2007), arXiv:nucl-ex/0608003 [nucl-ex].  
 [16] K. Slifer *et al.* (Resonance Spin Structure), Phys. Rev. Lett. **105**, 101601 (2010), arXiv:0812.0031 [nucl-ex].  
 [17] M. Gockeler, R. Horsley, D. Pleiter, P. E. L. Rakow, A. Schafer, G. Schierholz, H. Stuben, and J. M. Zanotti, Phys. Rev. **D72**, 054507 (2005), arXiv:hep-lat/0506017 [hep-lat].  
 [18] M. Posik *et al.* (Jefferson Lab Hall A), Phys. Rev. Lett. **113**, 022002 (2014), arXiv:1404.4003 [nucl-ex].  
 [19] J. Kodaira, S. Matsuda, T. Muta, K. Sasaki, and T. Uematsu, Phys. Rev. **D20**, 627 (1979).  
 [20] J. Kodaira, Nucl. Phys. **B165**, 129 (1980).  
 [21] J. Kodaira, S. Matsuda, K. Sasaki, and T. Uematsu, Nucl. Phys. **B159**, 99 (1979).  
 [22] R. L. Jaffe and X.-D. Ji, Phys. Rev. **D43**, 724 (1991).  
 [23] J. Blumlein and A. Tkabladze, Nucl. Phys. **B553**, 427 (1999), arXiv:hep-ph/9812478 [hep-ph].

TABLE I.

$Q^2$ GeV <sup>2</sup> /c <sup>2</sup>	x	Total	Measured	Elastic	Low x
$Q^2$	x	(total)	(measured)	(elastic)	(low-x)
$Q^2$		(total)	(measured)	(elastic)	(low-x)
$Q^2$		(total)	(measured)	(elastic)	(low-x)
$Q^2$		(total)	(measured)	(elastic)	(low-x)